

## EFFECT OF MICRO DIMPLE AND ELECTRICALLY CONDUCTING COUPLE STRESS FLUID IN EHL LINE CONTACTS

**SURESH JADHAV**

Assistant Professor, Department of Mechanical Engg. VJTI Matunga Mumbai, India.  
Email: jadhavsuresh1975@gmail.com

**GANANATH D. THAKRE**

Sr. Scientist, Advanced Tribology Research Centre, CSIR-IIP Dehradun, India. Email: gananath@gmail.com

**SATISH C. SHARMA**

Professor, Department of Mechanical and Industrial Engg. Tribology Laboratory IIT-Roorkee, India.  
Email: sshmefme@iitr.ac.in

### Abstract

This present study investigates the influence of micro textures and coupled fluid i.e. magneto hydrodynamic coupled stress fluid on the performances of EHL characteristics line contacts. Micro-textured of different shapes are provided on the contact surfaces operating with coupled fluid. The solution of Stokes micro-continuum for couple stress and modified Reynolds equation and magneto hydrodynamic fluid are combined to obtain mathematical model. The mathematical model has been solved with the finite element analysis technique. It has also been shown that a textured contact surface tends to lower the coefficient of friction. Providing micro textures on contact surfaces, remarkable enhance the performances of EHL characteristics line contacts. Couple fluid also significantly increases the contact surface's ability to support loads and inhibits the development of thin films, both of which could occur when surfaces are in contact with each other. Results show that the coupled stress and magnetic field effect, induced by micro dimples, has a remarkable influence on performances of EHL line contacts.

**Keywords:** EHL, Line Contact, Couple Stress Fluid, Magnetic Micro Dimples, Hartman Number, FEA

### Nomenclature

$b = 4R \sqrt{\frac{W}{2\pi}}$	Half Hertzian contact width (m)
$E'$	Effective elastic modulus of roller (Pa)
$h$	film thickness(m)
$H = hR/b^2$	Non- dimensional film thickness
$u_a$	Average rolling speed (m/s)
$V$	Linear velocity
$U = \eta_0 u / E'R$	Non- dimensional speed parameter
$\Omega = \frac{3U\pi^2}{4W^2}$	Speed factor
$p$	Pressure(Pa)
$\rho$	Density(kg/m <sup>3</sup> )
$P = p/P_h$	Non- dimensional pressure
$P_h = E'b/4R$	Maximum Hertzian pressure(Pa)
$G = \alpha E'$	Non-dimensional material parameter

$H = \frac{h R}{b^2}$	Non-dimensional Fluid film thickness
$H_{min}$	Non-dimensional minimum fluid film thickness
$H_{cent}$	Non-dimensional central fluid film thickness
R	Equivalent radius of contact(m)
w	Applied load per unit length (N/m)
$W = w/E'R$	Non-dimensional load parameter
z	Roeland's parameter
x	Abscissa along rolling direction(m)
$X = x/b$	Non-dimensional abscissa
$\Psi(h, l, H_m)$	Magneto hydrodynamic (MHD) couple stress function
$\bar{\eta}$	Dimensionless Viscosity
w	External load per unit width
$H_0$	Offset film thickness
cof	Coefficient of Friction
$\bar{h}_p$	Dimensionless micro texture depth
$\delta$	Dimensionless radius of micro textures
$r_p$	Base radius of micro texture mm
$w_L$	Width of rectangle micro textures
$x_{li}$	Input local co-ordinate of micro textures
X	Co-ordinates
$X_L$	Local co-ordinates
$H_{mt}$	Micro textures
$H_{mtpara}$	Parabolic micro textures mm
$H_{mttrapezoidal}$	Triangle micro textures mm
$H_m$	Hartmann number
lc	Couple stress parameter
$\sigma$	Electrical conductivity of the lubricant
$E_z$	Induced electric field in the z direction
$\vec{j}$	Current density
$\vec{F}_l$	Lorentz force
$B_o$	External magnetic field
$X_{in}$	Inlet boundary condition
$X_o$	Outlet boundary condition
W	Weighted function
$K_r^e(X)$	kernel
conv <sub>p</sub>	Pressure convergence
conv <sub>w</sub>	Load convergence
AMT	Artificial produced micro textures
sph	Spherical
rect	Rectangle
tri	Triangle
<i>Greek symbols</i>	
$\eta_0$	Inlet viscosity of the lubricant(pa-s)
$\eta = \frac{\eta}{\eta_0}$	Non-dimensional viscosity

$\rho = \frac{\rho}{\rho_0}$	Non-dimensional density
$q_x$	Flow rate
$V_1$	Velocity
$v_1$	Micro-rotation velocity
$H_0$	Central offset film thickness(m)
Matrices	
$[F]$	Fluidity matrix
$\{R\}$	Hydrodynamic term
$\{p\}$	Nodal pressure vector
$[J]$	Jacobian matrix

## 1. INTRODUCTION

Unprecedented advancements in technology over the last decade have led machines to work under increasingly stringent and rigorous working conditions. In order to create machines that are more accurate, efficient, and have a longer lifespan before failure, bearing designers are presented with a difficult problem. The effectiveness of the machine's bearings and the chosen lubricant are fully dependent on each other. Lubrication rheology technology has developed as a useful technique to enhance the characteristics of tribo-contacts with configurable dynamic properties for an upcoming generation of machines. Lubricants used in modern industrial applications frequently incorporate with polymeric additives. Das [1] presented a theoretical examination of EHL line contact lubrication utilising couple stress fluids. The findings revealed that the central film thickness increased with the coupling stress fluid parameter in EHL contacts lubricated with complex fluids, such as synthetic and polymeric fluids. Effects of couple stresses and surface roughness was studied by Rao et al. [2] on the minimum film thickness of heavily loaded rollers. According to the study, the EHL minimum film thickness increases as the chain length of the additive molecules increases. Additionally, the EHL minimum film thickness increases for transverse orientation of roughness while decreasing for longitudinal orientation of roughness. Akbarzadeh et al.[3] and Liu et al. [4] studied the running-in features of an EHL line contact. There is change in asperity heights due to the plastic deformation (experiencing both elastic and plastic contact) during the running-in process. Xiao et al. [5] and Torabi et al. [6] investigated the rough friction in lubricated sliding of roller surfaces (made to approximate real gear surfaces). They concluded that electrochemically deburred surfaces, which are competitive to fine-ground surfaces in lubricated rolling/sliding contact, possessed a lower friction coefficient. The influence of couple stress fluid was investigated by Sarangi et al. [7] and Saini et al.[8] On the EHL finite line contact. The study presented significant increase in the value of overall film thickness with couple stress parameter, which reduces the chances of metal-to-metal contact and thus tends to produce less wear. Additionally, the analysis indicates that the coefficient of friction decreases as the couple-stress parameter increases. In actual practice, the characteristics of the finishing processes controls the geometric shape of any engineering surfaces. The surface texturing enabled the development of desired surface profiles in order to enhance the EHL performance. Menezes et al. [9] investigated the effect of surface roughness on transfer layer development and the

coefficient of friction in a tin-steel tribo-system. Surface texture and roughness have been proven to have a significant influence on the formation of a transfer layer, the coefficient of friction, and the presence of stick-slip motion. To avoid abrupt changes in lubricant viscosity at high temperatures, high thermal and electrical conductivity lubricants blended with polymer additives have been employed. Mobil™ DTE 932 GT, widely available lubricant oil, has outstanding electrical conductivity [10], reduction in load carrying capacity caused by low viscosity can be mitigated by adding an external magnetic field. Magneto-fluid dynamics, magneto-hydrodynamics (MHD), or hydro-magnetics are the studies of electrically conducting fluids in the presence of a magnetic field. Furthermore, magnetic fields have several applications in research and industry, including crude oil purification, power generation, accelerators and propulsion. Numerous researchers [10, 11] have investigated the effect of a transverse magnetic field on the behaviour of an electrically conducting fluid in a fluid film bearing. In the literature, several theoretical and experimental research on the utilize MHD fluids in slider bearings [12], journal bearings [13, 14], and squeeze films [15, 16] have been published. However, the aforementioned investigations do not take into account lubricating surface deformation. According to a recent analysis, concentrated contacts work substantially better when the surface characteristics are clearly stated in terms of shape, size and orientation [17]. Micro dimples have been revealed to function as oil reservoirs in starved lubricated situations, which not only feed lubrication to the contact by smearing but also serve as wear particle traps [18]. The hydrodynamic lubrication of concentrated contacts can be influenced by the geometrical morphologies of dimples [19]. In terms of tribological behaviour, micro-textures have been shown to substantially improvement in the contacting surfaces in motion. Theoretical and experimental results that have been reported in literatures [20–23] have indicated significant benefits of micro textures in a variety of practical applications. A through scan of available literatures combined effect of micro-textures with different shapes (parabolic and trapezoidal) and coupled fluid i.e. couple stress magneto hydrodynamic fluid has not yet been studied in EHL conjunction. The author believes that the detailed computational analysis of EHL line contacts using micro-texture patterns and lubricated with coupled fluid has not yet been studied. In order to assess the cumulative consequences of micro textures and coupling fluid on the performance EHL features of line contacts, this research intends to investigate these two factors separately. To identify the most optimal characteristics of two micro-dimple shapes, parabolic and trapezoidal, parametric research is used.

## 2. MATHEMATICAL FORMULATION

The following subsections discuss the governing equations, including the density-pressure relation, fluid film thickness equation, modified Reynolds equation, load balance equation, viscosity-pressure relation and finite element formulation. Fig.1 represents schematic of EHL line contacts in the presence of externally applied magnetic field and micro textures i.e.a) trapezoidal and b) parabolic shape.

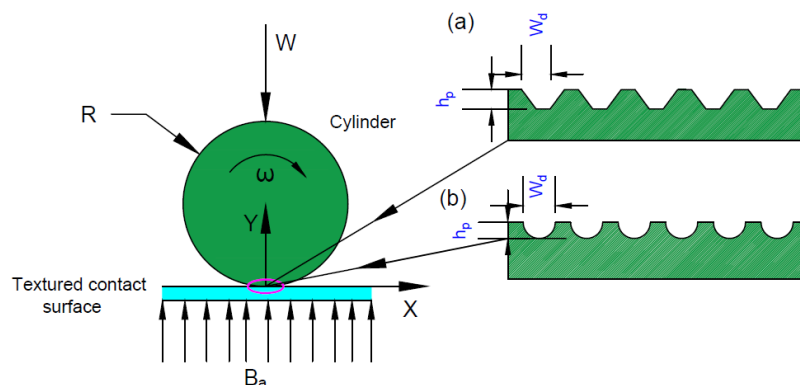


**Fig 1: schematic of EHL line contacts in the presence of externally applied magnetic field and micro textures a) trapezoidal and b) parabolic shape**

According to [24,10], the momentum equation and flow continuity for an electrically conducting couple stress lubricant that experiences a magnetic field is as follows:

$$\frac{\partial \rho}{\partial t} + \nabla \cdot (\rho \cdot \vec{v}) = 0 \quad (1)$$

$$\rho \left( \frac{\partial \vec{v}}{\partial t} + \vec{v} \cdot \nabla \vec{v} \right) = -\nabla \cdot p + \rho F' + \frac{1}{2} \rho \nabla \times M' + (\lambda + \mu + \eta \nabla^2) \nabla (\nabla \cdot \vec{v}) + (\mu - \eta \nabla^2) \nabla^2 \vec{v} + \vec{F}_l \quad (2)$$

An electrically conducting lubricant experiences the Lorentz force  $\vec{F}_l$  when a magnetic field ( $B_o$ ) is present, as illustrated in Eq. 2.

Lorentz force  $\vec{F}_l = \vec{J} \times \vec{B}$  is a type of body force that is expressed as: for steady flow  $\frac{\partial \rho}{\partial t} = 0$ ;

$\vec{J} = \sigma (\vec{E} + \vec{v} \times \vec{B})$  is constant for incompressible fluids  $\nabla \cdot \vec{v} = 0$  When body forces (excluding the Lorentz force), body couples and inertia forces are excluded, Eqs. (1) And (2) simplify as

$$\nabla \cdot \vec{v} = \frac{\partial u}{\partial x} + \frac{\partial v}{\partial y} = 0 \quad (3)$$

$$0 = -\nabla p + \mu \nabla^2 \vec{v} - \eta \nabla^4 \vec{v} + \vec{J} \times \vec{B} \quad (4)$$

The simplified form of the momentum equation (Eq. 4) is as follows:

$$\mu \frac{\partial^2 u}{\partial y^2} - \eta \frac{\partial^4 u}{\partial y^4} - \sigma B_o^2 u = \frac{\partial p}{\partial x} + \sigma E_z B_o$$

(5)

$$\frac{\partial p}{\partial y} = 0$$

(6)

$E_z$  denotes the components of the induced electric field in the z direction. It is usually considered that the contact surfaces are perfect insulators. With zero net current flow, the electric field in Eq. 5 as:

$$\int_0^h (E_z + u B_o) dy = 0;$$

(7)

The B.Cs. are stated as follows:

$$\text{For } y=0; \left( u = U; v = \frac{\partial h}{\partial t} \right)_{\text{No slip}}; y=h; (v=0; u=0) \quad \text{and} \quad \left( \frac{\partial^2 u}{\partial y^2} = 0 \right)_{\text{No couplestress}}$$

(8)

The fluid's velocity in the x direction can be determined by integrating Eq. (5) using the aforementioned boundary condition (Eq. 8).

$$u = -\frac{U}{2} \left( \frac{\delta^2}{\gamma^2 - \delta^2} \left( \frac{\sinh\left(\frac{\gamma h}{1}\right) - \sinh\left(\frac{\gamma y}{1}\right) + \sinh\left(\frac{\gamma(h-y)}{1}\right)}{\sinh\left(\frac{\gamma h}{1}\right)} \right) - \left( \frac{\gamma^2}{\gamma^2 - \delta^2} \left( \frac{\sinh\left(\frac{\delta h}{1}\right) - \sinh\left(\frac{\delta y}{1}\right) + \sinh\left(\frac{\delta(h-y)}{1}\right)}{\sinh\left(\frac{\delta h}{1}\right)} \right) \right) \right) \quad (9)$$

$$- \frac{h_0^2 h}{2\mu H^2} \frac{\partial p}{\partial x} \left( \frac{1}{\frac{\delta^2}{\gamma} \tanh\left(\frac{\gamma h}{2l}\right) - \frac{\gamma^2}{\delta} \tanh\left(\frac{\delta h}{2l}\right)} \right) \left( \frac{\sinh\left(\frac{\gamma h}{1}\right) - \sinh\left(\frac{\gamma y}{1}\right) - \sinh\left(\frac{\gamma(h-y)}{1}\right)}{\sinh\left(\frac{\gamma h}{1}\right)} - \gamma^2 \frac{\sinh\left(\frac{\delta h}{1}\right) - \sinh\left(\frac{\delta y}{1}\right) - \sinh\left(\frac{\delta(h-y)}{1}\right)}{\sinh\left(\frac{\delta h}{1}\right)} \right)$$

$$\gamma = \left( \left( 1 + \sqrt{1 - \left( \frac{4l^2 H_m^2}{h_0^2} \right)} \right) / 2 \right)^{1/2}; \quad \delta = \left( \left( 1 - \sqrt{1 - \left( \frac{4l^2 H_m^2}{h_0^2} \right)} \right) / 2 \right)^{1/2}; \quad l = (\eta/\mu)^{1/2} \quad (10)$$

Where the lubricant's couple stress additives' characteristic length,  $l$ , is indicated. Non-dimensional constants include  $\gamma$  and  $\delta$ .  $H_m$  is the Hartmann number, which can be used to compare the strength of the electro-magnetic force to the viscous force  $H_m = B_o h_o (\sigma/\mu)^{1/2}$ ,  $\sigma$  for the lubricant's electrical conductivity. The result is obtained by substituting the velocity from Equation 9 into Equation 3 for continuity.

$$\frac{\partial}{\partial x} \left( \frac{h^3}{12\mu} \Psi(h, l, H_m) \frac{\partial p}{\partial x} \right) = \frac{\Omega}{2} \frac{\partial h}{\partial x} \quad (11)$$

Where  $\Psi(h, l, H_m) = \left( \frac{6h_0^2}{hlH_m^2} \right) \left( \frac{\gamma^2 - \delta^2}{\left( \frac{\gamma^2 \tanh\left(\frac{\delta h}{2l}\right) - \delta^2 \tanh\left(\frac{\gamma h}{2l}\right) \right) - \frac{2l}{h}} \right)$  is MHD couple stress function (12)

Without accounting for the hydrodynamic term, the behaviour of an EHL line contact can be studied using Equation (11), a modified Reynolds equation that describes a couple-stress lubricant under the effect of an externally provided magnetic field ( $B_o$ ). In limiting conditions, the magneto-fluid dynamics couple stress function (Eq. 12) simplifies to these criteria:

Case A: As,  $l \rightarrow 0$  flow equation is reduced to electrically conducting lubricant[10] i.e.

$$\lim_{l \rightarrow 0} \Psi(h, l, H_m) = \frac{6h_0^2}{h^2 H_m^2} \left( \frac{H_m h}{h_0} \coth\left(\frac{H_m h}{2h_0}\right) - 2 \right) \quad (13)$$

Case B: As,  $H_m \rightarrow 0$ , couple stress lubricant is reduced by the flow equation[25] i.e.

$$\lim_{H_m \rightarrow 0} \Psi(h, l, H_m) = 1 - \frac{12l^2}{h^2} + \frac{24l^3}{h^3} \tanh\left(\frac{h}{2l}\right) \quad (14)$$

Case C: As, both  $H_m, l \rightarrow 0$ , Newtonian lubricant is used to simplify the flow equation.

$$\lim_{H_m, l \rightarrow 0} \Psi(h, l, H_m) = 1 \quad (15)$$

Utilising the dimensionless parameters:

$$X = x/a; P = p/p_h; H = hR/a^2; \bar{p} = p/p_o; \bar{\eta} = \eta/\eta_o \quad (16)$$

The modified Reynolds equation is written in non-dimensional form as:

$$\frac{d}{dX} \left( \frac{\bar{p} H^3}{\bar{\eta}} \Psi(\bar{h}, \bar{l}, H_m) \frac{dP}{dX} \right) = \Omega \frac{d(\bar{p} H)}{dX} \quad (17)$$

$$\text{Where, } \Psi(\bar{h}, \bar{l}, H_m) = \frac{12}{\bar{h} H_m^2} \left( \frac{\gamma^2 - \delta^2}{\left( \frac{\gamma^2 \tanh\left(\frac{\delta \bar{h}}{\bar{l}}\right) - \delta^2 \tanh\left(\frac{\gamma \bar{h}}{\bar{l}}\right) \right) - \frac{\bar{l}}{H_m}} \right); \Omega = 3U\pi^2/4W^2 \quad (18)$$

The non-dimensional 1D modified Reynolds equation (Eq. 17) has been solved using FEM. It is assumed that the fluid pressure at the input and outflow of the EHL conjunction is equal to the ambient pressure. Due to the following boundary conditions (B.C), As a result, the Reynolds equation for pressure is solved.

Inlet B.C.

$$P = 0 \text{ at } P = X_{in} \quad (19)$$

Outlet B.C.

$$P = \frac{dP}{dX} \text{ at } X = X_o \quad (20)$$

## 2.1 Fluid Film Thickness Equation

To account for the artificial micro-textures (dents with parabolic and triangular shapes), the fluid film thickness in this study has been modified and is represented as follows:

$$H = H_0 + \frac{X^2}{2} - \frac{1}{\pi} \int_{-\infty}^{\infty} \ln|X - X'| |P(X')| dX' + H_{mt} \quad (16)$$

Hence, for artificial micro-texture shape,  $H_{mt}$  stands for the fluid film thickness component.

For the selected micro-textures (parabolic and trapezoidal) the term  $H_{mt}$  takes the form as,

$$H_{mtpara} = \bar{h}_p \left( 1 - \left| \frac{X_{Li} - X + r_p}{r_p} \right| \right)^2 \quad \text{if } X_L \leq r_p \quad (17)$$

$$H_{mtpara} = 0 \quad \text{if } X_L > r_p \quad (18)$$

$$H_{mttrap} = 2 * \bar{h}_p \left( 1 - \left| \frac{X_{Li} - X + r_p}{r_p} \right| \right) \quad \text{if } X_L \leq r_p \quad (19)$$

$$H_{mttrap} = 0 \quad \text{if } X_L > r_p \quad (20)$$

## 2.2 Density-Pressure Relation

The dimensionless form of the density-pressure relation is as follows:

$$\bar{\rho} = \left( 1 + \frac{0.6 \times 10^{-6} P. P_h}{1 + 1.7 \times 10^{-9} P. P_h} \right) \quad (21)$$

## 2.3 Viscosity-Pressure Relation

The dimension form of the viscosity-pressure relation is expressed as

$$\bar{\eta} = \exp((\ln \eta_0 + 9.67) \{-1 + (1 + 5.1 \times 10^{-9} P. P_h)^2\}) \quad (22)$$

## 2.4 Load Balance Equation

The load applied is supported by the pressure that has built up within the lubricant layer, thus the pressure derived from the Reynolds equation ought to satisfy the load balance condition.

$$\int_{x_i}^{x_o} p dx = w \quad (23)$$

Equation (25) is written in non-dimensional as:

$$\int_{x_i}^{x_o} PdX = \frac{\pi}{2} \quad (24)$$

## 2.5 Coefficient of Friction

In order to determine the pressure distribution and film shape, the governing equations have to be solved. These results are used to determine the coefficient of friction, which is written as [7].

$$\mu = \frac{\int_{x_{in}}^{x_o} \tau_b dx}{w} = \frac{\int_{x_{in}}^{x_o} \frac{h}{2} \left( \frac{dp}{dx} \right) dx}{w} \quad (25)$$

The corresponding dimensionless form is

$$\mu = - \sqrt{\frac{8W}{\pi^3}} \int_{x_{in}}^{x_o} H \left( \frac{dP}{dX} \right) dX \quad (26)$$

## 2.6 Finite Element Analysis

As shown in Fig. 1, a roller/cylinder on a flat surface has been utilised to model the EHL line contact problem in this study. Fluid film thickness, the modified Reynold's equation, and the load balance equation have all been discretized utilizing the Galerkin technique. A one-dimensional EHL line contact problem's fluid flow field was discretized using two noded linear isoparametric elements. In the lubricant flow field from the grid convergence investigation, the domain relevant to the study has been meshed from  $X_{inlet} = -5$  to  $X_{outlet} = 2.5$  with uniform optimise grid size of 450 elements is presented in Fig. 2. The two noded linear isoparametric elements were interpolated using the Lagrangian interpolation function [].

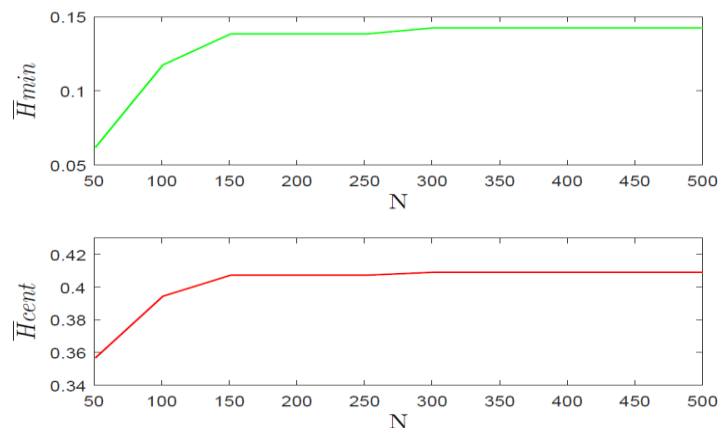


**Fig 2: Mesh sensitivity test with total number of nodes (N)**

The residue from equation (12) is expressed as:

$$R^e = \frac{\partial}{\partial \bar{x}} \left[ \frac{\bar{\rho} \bar{h}^3}{\bar{\eta}} \Psi(\bar{h} H) \frac{\partial \bar{p}}{\partial \bar{x}} \right] - \Omega \frac{\partial(\bar{\rho} \bar{h})}{\partial \bar{x}} \quad (27)$$

By multiplying the weighting function by its integral and equating it to zero, the Galerkin method is employed to reduce the residual.

$$\int_{\Omega^e} W R_i^e dx = 0 \quad (28)$$

$$\int_{\Omega^e} W \frac{\partial}{\partial \bar{x}} \left[ \frac{\bar{\rho} \bar{h}^3}{\bar{\eta}} \Psi(\bar{h} H) \frac{\partial \bar{p}}{\partial \bar{x}} \right] dx - W \Omega \frac{\partial(\bar{\rho} \bar{h})}{\partial \bar{x}} dx = 0 \quad (29)$$

Any two functions ( $f_1, f_2$ ) can be differentiated.

$$\frac{d(f_1 f_2)}{dx} = f_1 \frac{df_2}{dx} + f_2 \frac{df_1}{dx} \quad (30)$$

Using equation (30), equation (29) is transformed to,

$$\sum_{\Gamma} \left( \frac{W \bar{\rho} \bar{h}^3}{\bar{\eta}} \Psi(\bar{h} H) \frac{\partial \bar{p}}{\partial \bar{x}} \right) - \int_{\Omega^e} \frac{\bar{\rho} \bar{h}^3}{\bar{\eta}} \Psi(\bar{h} H) \frac{\partial \bar{p}}{\partial \bar{x}} \frac{\partial W}{\partial \bar{x}} d\bar{x} - \Omega \sum_{\Gamma} (W \bar{\rho} \bar{h}) + \Omega \int_{\Omega^e} \frac{\bar{\rho} \bar{h} \partial(W)}{\partial \bar{x}} d\bar{x} = 0 \quad (31)$$

The shape function of the primary variable, i.e, Pressure, replaces the weighted function  $W$  in this method. Therefore, an approximation of the solution is

$$\bar{p} = \sum_{i=1}^{p^e+1} N_i \bar{p}_j \quad (32)$$

$$N_1(\xi) = \frac{1-\xi}{2} \text{ and } N_2(\xi) = \frac{1+\xi}{2} \quad (33)$$

$$\sum_{j=1}^2 \left[ \int_{\Omega^e} \left[ \frac{\bar{\rho} \bar{h}^3}{12 \bar{\eta}} \Psi(\bar{h} H) \frac{\partial N_i}{\partial \bar{x}} \frac{\partial N_j}{\partial \bar{x}} dx \right] \bar{p}_j \right] = \frac{\Omega}{2} \int_{\Omega^e} (\bar{\rho} \bar{h}) \frac{\partial N_i}{\partial \bar{x}} dx + \sum_{\Gamma} \frac{W \bar{\rho} \bar{h}^3}{12 \bar{\eta}} \Psi(\bar{h} H) \frac{\partial N_j}{\partial \bar{x}} \bar{p}_j - \frac{\Omega}{2} \sum_{\Gamma} (N_i \bar{\rho} \bar{h}) \quad (34)$$

When pressure ( $\bar{p}$ ) over inter-element boundaries is taken into account as a boundary condition and a continuity condition equation (34) as:

$$[F_{ij}^e] \{ \bar{p}_j^e \} = \Omega \{ R_i^e \} \quad (35)$$

Where

$$[F_{ij}^e] = \int_{\Omega^e} \left[ \frac{\bar{\rho} \bar{h}^3}{12 \bar{\eta}} \Psi(\bar{h}, H) \frac{\partial N_i}{\partial \bar{x}} \frac{\partial N_j}{\partial \bar{x}} dx \right] \quad (36)$$

Elemental matrix equations (Eq.35) have been developed for each element and assembled to form a global system of equations, which is stated in matrix form as.

$$\begin{bmatrix} \bar{F}_{11} & \bar{F}_{12} & \dots & \bar{F}_{1j} & \dots & \bar{F}_{1n} \\ \bar{F}_{21} & \bar{F}_{22} & \dots & \bar{F}_{2j} & \dots & \bar{F}_{2n} \\ \vdots & \vdots & \vdots & \vdots & \vdots & \vdots \\ \bar{F}_{i1} & \bar{F}_{i1} & \dots & \bar{F}_{ij} & \dots & \bar{F}_{in} \\ \vdots & \vdots & \vdots & \vdots & \vdots & \vdots \\ \bar{F}_{n1} & \bar{F}_{n2} & \dots & \bar{F}_{nj} & \dots & \bar{F}_{nn} \end{bmatrix} \begin{bmatrix} \bar{p}_1 \\ \bar{p}_2 \\ \vdots \\ \bar{p}_{oi} \\ \vdots \\ \bar{p}_n \end{bmatrix} = \begin{bmatrix} \bar{R}_i^e \\ \bar{R}_i^e \\ \vdots \\ \bar{R}_i^e \\ \vdots \\ \bar{R}_i^e \end{bmatrix} \quad (38)$$

By adding a new kernel [29, 30] for elastic deformation, the film thickness equation is obtained as.

$$H(X) = H_0 + \frac{X^2}{2} - \frac{1}{\pi} \sum_{e=1}^N \int \ln|X - X'| \sum_{i=1}^{p^e+1} N_i \bar{p}_i(X') dX' \quad (39)$$

$$H(X) = H_0 + \frac{X^2}{2} - \frac{1}{\pi} \sum_{e=1}^N \sum_{i=1}^{p^e+1} K_i^e(X) \bar{p}_i^e \quad (40)$$

Where  $K_i^e(X)$  is the kernel expressed as:

$$\begin{aligned} K_i^e(X) &= \int \ln|X - X'| N_i^e(X') dX' \\ &= \frac{h^e}{2} \sum_{i=1}^m (\ln |X - X'(\xi_i)| N_i^e(\xi_i)) w_i \end{aligned} \quad (41)$$

When X is outside of e, Gaussian quadrature can be used to compute  $K_i^e(X)$  numerically.

The discretization of the load balance equation is as follows [31, 32]:

$$\sum_{e=1}^N \sum_{i=1}^{p^e+1} p_i^e N_i^e(X) dX - \frac{\pi}{2} = 0 \quad (42)$$

The load balance equation using Gaussian quadrature is,

$$\sum_{e=1}^N \sum_{i=1}^{p^{e+1}} p_i^e N_i^e |J|W - \frac{\pi}{2} = 0 \quad (43)$$

The discretized coefficient of friction is

$$\mu = -\sqrt{\frac{8W}{\pi^3}} \sum_{e=1}^N \sum_{i=1}^{p^{e+1}} H P_i^{e+1} \frac{dN_i^e(X)}{dX} dX = 0 \quad (44)$$

Gaussian quadrature is employed to express the coefficient of friction as

$$\mu = -\sqrt{\frac{8W}{\pi^3}} \sum_{e=1}^N \sum_{i=1}^{p^{e+1}} H P_i^e \frac{dN_i^e}{dX} |J|W \quad (45)$$

### 3. SOLUTION PROCEDURE

Using the finite element method, fluid film thickness equation, load balance equation and modified Reynolds equation have been developed in the part preceding. The solution process used in the present instance is depicted in Fig. 2 EHL contact solution scheme, on the basis of the analysis and formulation presented in the preceding part. The primary steps taken to create a reliable and efficient numerical FEM solver are outlined below.

1. The solution domain is discretized using two-noded linear isoparametric elements.
2. Using the Hertzian pressure distribution, fluid film pressure is initialised.
3. Using equations (21) and (22), density and viscosity are calculated (given a starting pressure i.e. Hertzian pressure).
4. Calculating the thickness of a fluid film while taking into account elastic deformation and offset film thickness.
5. Using the Gaussian quadrature numerical integration method, compute the matrices and vectors of the elemental fluidity.
6. Consolidation of elemental fluidity matrices and vectors into global fluidity matrices.
7. Using global fluidity matrices with boundary limitations.
8. Linearized system of equations for lubricant layer pressure distribution computation utilising GMRES technique.
9. Continue performing steps 3–8 until the pressure convergence condition is achieved.

Pressure convergence

$$\text{conv}_p = \frac{|\sum p_i|_{n+1} - |\sum p_i|_n}{|\sum p_i|_n} \leq 1.0 \times 10^{-5} \quad (40)$$

10. Calculating the central offset lubricant layer thickness and load balance equation's residual.
11. Repeat steps 3–10 until the load balance convergence condition is satisfied.

Load convergence

$$\text{conv}_w = \frac{\sum \text{Load} - \pi/2}{\sum \text{Load}^n - \sum \text{Load}^{n-1}} \leq 1.0 \times 10^{-5} \quad (41)$$

12. Once the convergence conditions have been achieved, compute fluid film pressure fluid film distribution utilizing the formulas described in the preceding sections.

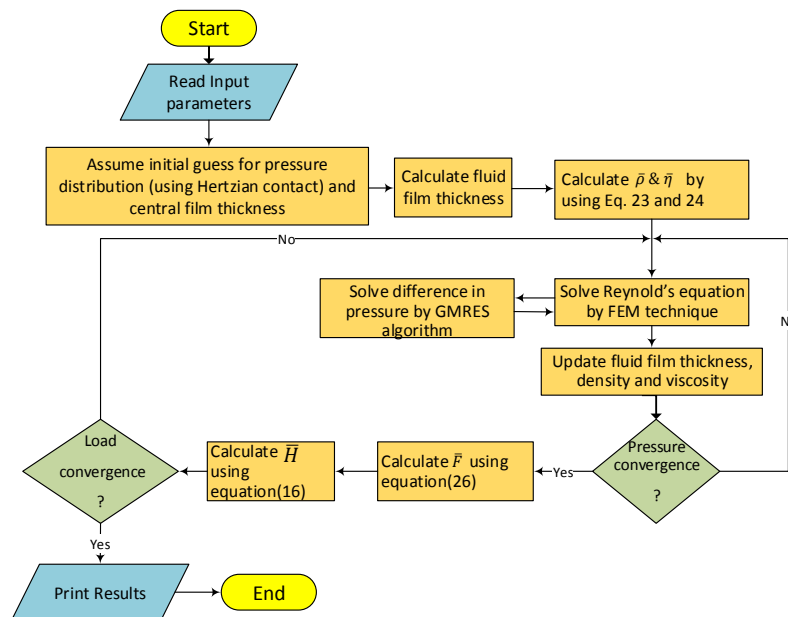


Fig 3: solution scheme of EHL contact

#### 4. NUMERICAL MODEL VALIDATION

MATLAB R2013b software was used to create a computer program for computing elastic deformation and nodal fluid film pressure. For the solution of EHL line contact, the finite element analysis technique was successfully utilised. However, in order to rely on the accurateness of simulated results, the program has to be extensively validated. As a result, the  $\bar{H}_{min}$  thickness values generated from the created code were compared and validated with results [33, 34]. Table 1 compares the results obtained from the current numerical model with those obtained from [33, 34]. The little variance in results (1-5%) can be attributed to the two research' distinct solution schemes. It is allowed to compute the results notwithstanding the very minor deviation. As a result, it is possible to draw the conclusion that the model created for this study is valid based on the comparative assessment.

**Table 1: Influence of dimensionless load, speed and material parameters on minimum fluid film thickness ( $\bar{H}_{min}$ ) of EHL line contact**

S. No.	Dimensionless Load parameter (W)	Dimensionless Speed parameter (U)	Dimensionless Material parameter (G)	Least Squares Fit Formula			Dowson Empirical Formula			EHL Theory		
				Present $\bar{H}_{min}$	Hamrock and Jacobson [30] $\bar{H}_{min}$	% Error	Present $\bar{H}_{min}$	Hamrock and Jacobson [30] $\bar{H}_{min}$	% Error	Present $\bar{H}_{min}$	Hamrock and Jacobson [30] $\bar{H}_{min}$	% Error
1	1.64E-05	1.00E-11	5000	2.03E-05	2.05E-05	1.25E+00	2.03E-05	2.20E-05	8.02E+00	2.03E-05	2.03E-05	0.359128
2	2.05E-05	1.00E-11	5000	1.99E-05	2.00E-05	7.25E-01	1.99E-05	2.14E-05	7.12E+00	1.99E-05	1.97E-05	-0.79651
3	2.46E-05	1.00E-11	5000	1.95E-05	1.96E-05	3.77E-01	1.95E-05	2.09E-05	6.45E+00	1.95E-05	1.94E-05	-0.75273
4	3.00E-05	1.00E-11	5000	1.92E-05	1.92E-05	-5.21E-03	1.92E-05	2.04E-05	5.72E+00	1.92E-05	1.92E-05	-0.01042
5	2.05E-05	2.00E-11	5000	3.16E-05	3.27E-05	3.34E+00	3.16E-05	3.47E-05	8.94E+00	3.16E-05	3.34E-05	5.161252
6	2.05E-05	3.00E-11	5000	4.15E-05	4.37E-05	4.92E+00	4.15E-05	4.62E-05	1.01E+01	4.15E-05	4.30E-05	3.530177
7	4.01E-05	1.96E-11	2553.7	2.13E-05	2.04E-05	4.18E+00	2.13E-05	2.18E-05	2.53E+00	2.13E-05	2.02E-05	-5.54674
8	4.01E-05	5.60E+00	3591.1	5.03E-05	5.23E-05	3.82E+00	5.03E-05	5.47E-05	8.13E+00	5.03E-05	5.25E-05	4.224601

## 5. RESULT AND DISCUSSION

The influence of each dimensionless design parameter, such as the dimensionless speed, load, and material parameter, as well as the artificial micro texture geometry (parabolic and trapezoidal) and the magneto hydrodynamic (MHD) fluid, on the EHL performance characteristics of line contacts has been investigated through a parametric investigation. The influence of externally served as magnetic fields on the properties of EHL line contact can be seen in the Hartmann number ( $H_m$ ) of MHD fluid. Eq. (9) becomes the classical Reynolds equation when  $H_m$  approaches 0, resulting in the lubricant being considered as operating according to a Newtonian fluid (i.e., a non-conducting electrical lubricant). Table 2 shows the operating variables considered for this analysis from the existing literature [1, 8, 7, 35-37]. The coupled solution of film thickness equation (16), load balance equation (24), Reynolds equation (9) and fluid rheology equation (21,22) fulfilling the boundary conditions and utilising finite element analysis approach yields a steady state lubricant film pressure distribution. The influence of abovementioned parameters is presented on the non-dimensional performance indicators such as  $\bar{H}_{cent}$  and  $\bar{H}_{min}$  film thickness, fluid film thickness profile, pressure distribution profile and coefficient of friction profile etc. in the succeeding sub sections.

**Table 2: Numerical data for present study**

a) Lubricant rheological properties[1,7,8,32-34]		
Physical quantity	symbol	Numerical Value of Physical quantity
Lubricant viscosity	$\eta$	1.55 mPa.s
Applied magnetic field	$B_0$	0~2.25Wb/m <sup>2</sup>
Couple stress parameter	lc	$2 \times 10^{-5} - 4 \times 10^{-5}$
Hartmann number (range)	Hm	0-10
Electrical conductivity(	$\sigma$	$1.0710 \times 10^6 mho/m$
b) The ranges of dimensionless speed, load and material parameters used herein are specified in[1,32]		
Dimensionless load	$\bar{W}$	$2 \times 10^{-5} - 7 \times 10^{-5}$
Dimensionless speed	$\bar{U}$	$2 \times 10^{-11} - 7 \times 10^{-11}$
Material parameter	G	5000

## 5.1 Effect of electrical conducting couple stress fluid parameters and micro dimples

### 5.1.1 Fluid film and pressure distribution

Figure 3 compares the fluid film and pressure distribution profile, of Newtonian fluid ( $lc=0$ ;  $Hm=0$ ) with ECSF at different parameter. Figure 4 indicates that the pressure spike eventually decreases and the fluid film rises when compared to Newtonian fluid. This can be attributed that the pressure spike reduction caused by fluid film thickening. Fluid film thickness obtained using ECSF parameter is higher than that for Newtonian fluid ( $lc=0$ ;  $Hm=0$ ). Quantitatively, central ( $\bar{H}_{cent}$ ) and minimum ( $\bar{H}_{min}$ ) fluid film thickness enhanced by a maximum of 36.45% and 35.35% by employing with electrically conducting couple stress fluid parameter ( $lc=4 \times 10^{-5}$ ;  $Hm=4$ ). Fig.3 depicts the fluid film and contact rippling pressure profile for micro dimples, electrically conducting couple stress fluid parameters and Newtonian fluid lubricated EHL contact. The results clearly show that micro dimples, ECSF characteristics have a beneficial effect on the fluid film and pressure distribution profile. The presence of applied magnetic field and long chain polymer additives and textures contact surfaces with trapezoidal shape ( $Hm=4$ ;  $lc=4 \times 10^{-5}$ ; Trape) bounds to increases  $\bar{H}_{cent}$  and  $\bar{H}_{min}$  fluid film of 48.33% and 44.28% and reduce the pressure spike of 19.23 % compared to the Newtonian fluid ( $lc=0$ ;  $Hm=0$ ). The existence of the film thickness constriction as well as the resulting localised and abrupt change in the flow component's velocity, in both direction and magnitude, result in a pressure spike. Following a spike, pressure gradually reduces to ambient pressure, resulting in film break-up and cavitation. Finally, the minimum film thickness is influenced by the outflow zone and the characteristics of lubrication in that region. To be more specific, it affects the degree of variation between the  $\bar{H}_{cent}$  and  $\bar{H}_{min}$  fluid film, which is the depth of the film thickness constriction. A comprehensive analysis of the fluid film thickness increase percentage for micro dimples (parabolic and trapezoidal) under various operating conditions is presented in Tables 3 and 4.

**Table 3: Percentage (%) variation in dimensionless minimum fluid film thickness ( $\bar{H}_{min}$ ) of EHL line contacts due to electrically conducting lubricant blended with additives (ECL) and micro textures**

Sr. no.	Parameters	U=3e-11;W=2e-5;G=5000		U=3e-11;W=4E-5;G=5000		U=4e-11;W=2E-5;G=5000		U=6e-11;W=2E-5;G=5000	
		$\bar{H}_{min}$	% change	$\bar{H}_{min}$	%change	$\bar{H}_{min}$	%change	$\bar{H}_{min}$	%change
1	Smooth	0.622614	0.00	0.229824	0.00	0.641601	0.00	0.840257	0.00
2	Trapezoidal	0.684875	10.00	0.252806	10.00	0.711146	10.83933	0.935282	11.30912
3	Parabolic	0.741209	19.04799	0.272197	18.43748	0.776628	21.04533	1.02174	21.59853
4	ECLCS HM=3;lc=3e-5	0.918451	47.51533	0.310262	35.00021	0.884962	37.93023	1.239825	47.55312
5	Trapezoidal	1.021296	64.0336	0.34215	48.8748	0.992079	54.62554	1.390994	65.54398
6	Parabolic	1.126141	80.87311	0.3734	62.47215	1.056063	64.59803	1.480884	76.2419
7	ECLCS HM=5;lc=5e-5	1.193986	91.76992	0.403341	75.50027	1.190495	85.55064	1.669193	98.65278
8	Trapezoidal	1.327685	113.2437	0.444794	93.53724	1.343372	109.3781	1.882054	123.9856
9	Parabolic	1.463983	135.135	0.485419	111.2138	1.419348	121.2198	1.990308	136.8691

$$\% \text{change} = \left( \frac{(\bar{H}_{\min})_{ECLCS,smooth,texture(\bar{W},\bar{U})} - (\bar{H}_{\min})_{NCL,smooth(\bar{W},\bar{U})}}{(\bar{H}_{\min})_{NCL,smooth(\bar{W},\bar{U})}} \right)$$

**Table 4: Percentage (%) variation in dimensionless central fluid film thickness ( $\bar{H}_{\text{cent}}$ ) of EHLcontacts due to electrically conducting lubricant mixed additives (ECL) and micro textures**

Sr. no.	Parameters	W=2e-5;U=2e-11; G=5000		W=5E-5;U=2e-11; G=5000		U=4e-11;W=2e-5;G=5000		U=6e-11;W=2e-5;G=5000	
		$\bar{H}_{\text{cent}}$	%change	$\bar{H}_{\text{cent}}$	%change	$\bar{H}_{\text{cent}}$	%change	$\bar{H}_{\text{cent}}$	%change
1	Smooth	0.77068	0.00	0.280733	0.00	0.711146	0.00	0.935282	0.00
2	Trapezoidal	0.933186	21.08614	0.338207	20.47262	0.776628	9.207925	1.02174	9.243993
3	Parabolic	1.012293	31.35069	0.366612	30.59078	0.87159	22.56128	1.135986	22.45914
4	ECLCS Hm=3;lc=3e-5	1.332365	72.88177	0.411271	46.49872	1.096752	54.22321	1.53687	64.32153
5	Trapezoidal	1.443395	87.28859	0.44738	59.36139	1.220632	71.64296	1.710088	82.84189
6	Parabolic	1.554426	101.6954	0.482099	71.72848	1.333765	87.5514	1.868441	99.77301
7	ECLCS Hm=5;lc=5e-5	1.598838	107.4581	0.493525	75.79846	1.447713	103.5746	2.028668	116.9044
8	Trapezoidal	1.732074	124.7463	0.536856	91.23367	1.611235	126.5687	2.257316	141.3513
9	Parabolic	1.865311	142.0345	0.578519	106.0742	1.708302	140.2181	2.393829	155.9472

$$\text{Percentage change} = \left( \frac{(\bar{H}_{\text{cent}})_{ECLCS,smooth,texture(\bar{W},\bar{U})} - (\bar{H}_{\text{cent}})_{smooth(\bar{W},\bar{U})}}{(\bar{H}_{\text{cent}})_{smooth(\bar{W},\bar{U})}} \right)$$

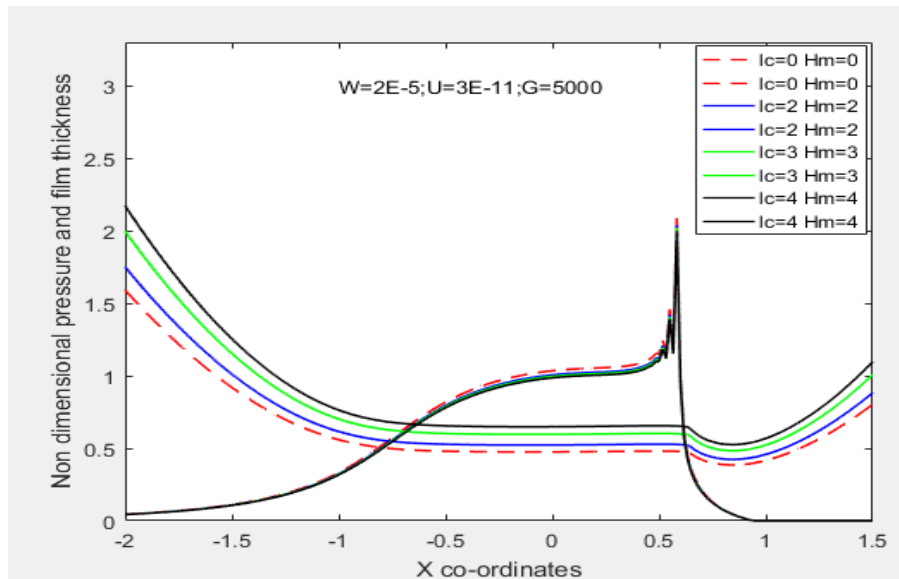


**Fig 3: Effect of electrically conducting couple stress fluid parameter on pressure and fluid film thickness profile at  $W=3 \times 10^{-5}$ ;  $U=2 \times 10^{-11}$ ;  $G=5000$**

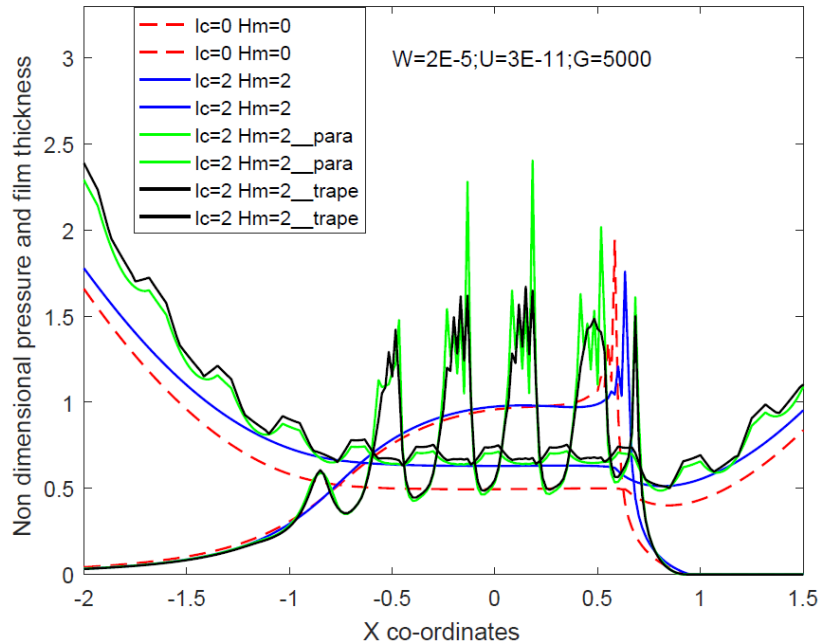


**Fig 4: Effect of ECSF parameter and different geometry of dimple on pressure and fluid film thickness profile at  $W=2 \times 10^{-5}$ ;  $U=3 \times 10^{-11}$ ;  $G=5000$**

### 5.1.2 Minimum ( $H_{min}$ ) and central ( $H_{cent}$ ) fluid film thickness

Effect of electrical conducting couple stress fluid parameters and micro dimples shapes (parabolic and trapezoidal) on  $H_{min}$  and  $H_{cent}$  fluid film thickness are illustrated through Fig.5 and Fig 6. Minimum ( $H_{min}$ ) and central ( $H_{cent}$ ) fluid film thickness rise with the electrical conducting couple stress fluid parameters ( $Hm=2;lc=2;para$ ) and micro dimples shapes (trapezoidal) among other micro dimple shape and Newtonian fluid ( $Hm=0;lc=0;parabolic$ ). The percentage increment of  $H_{min}$  and  $H_{cent}$  fluid film thickness are 54.33% and 58.65%. Moreover, the presence of textured contact surface provides higher value of minimum fluid film thickness than smooth surface for Newtonian lubricant and the value of minimum fluid thickness is pronounced for the lubrication with electrical conducting couple stress fluid parameters. The reason behind such a behavior is that the textured surface provides lower value of maximum fluid pressure and the pronounced effect due to electrical conducting couple stress fluid parameters can be accredited to aligning nature of suspended magnetic particles under the application of externally applied magnetic field and along the long chain polymer additives. Tables 3 and 4 show comprehensive comparisons with percentage increase in fluid film thickness under varied operating conditions for micro dimples (parabolic and trapezoidal).

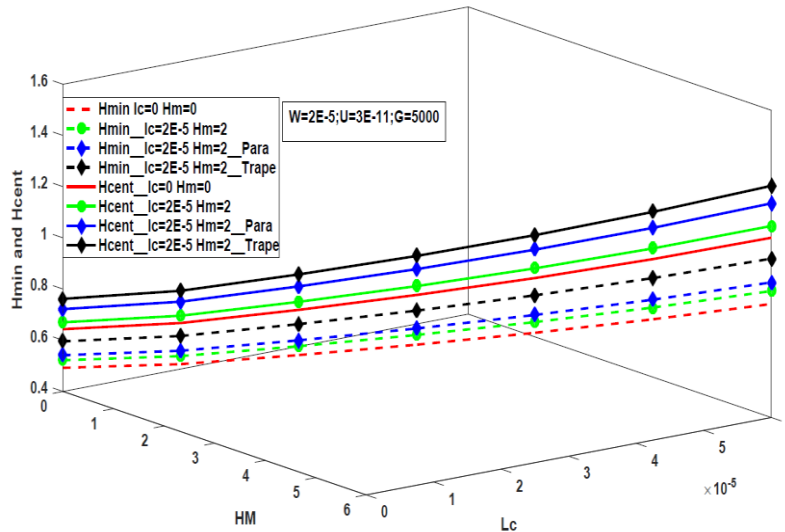


**Fig 5: Effect of ECSF parameter and different geometry of dimple on minimum and central fluid film thickness at  $W=2 \times 10^{-5}$ ;  $U=3 \times 10^{-11}$ ;  $G=5000$**

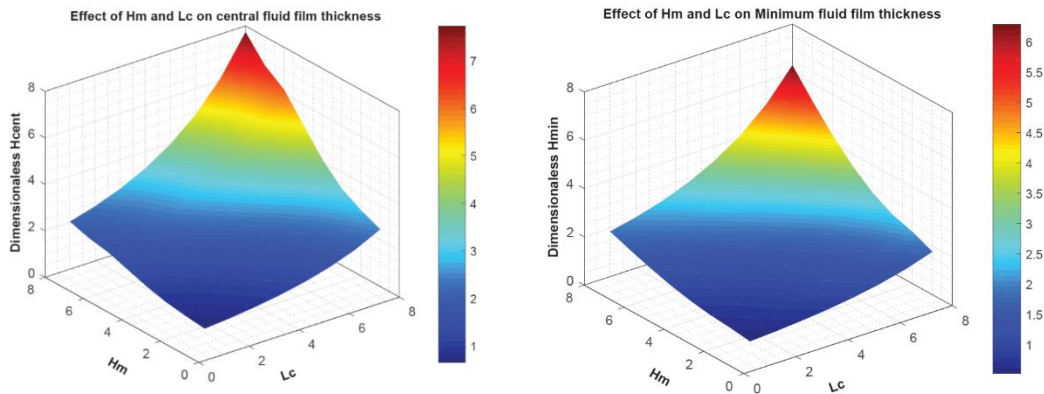


**Fig 6: Effect of ECSF parameter and different geometry of dimple on (a) central and (b) minimum fluid film thickness; at  $W=2 \times 10^{-5}$ ;  $U=3 \times 10^{-11}$ ;  $G=5000$**

### 5.1.3 Coefficient of friction ( $\bar{\mu}$ )

Effect of micro dimples, electrically conducting couple stress fluid parameters and Newtonian fluid on coefficient of friction ( $\bar{\mu}$ ) are presented in Fig.7. It can be observed from 3D plot that the friction coefficient ( $\bar{\mu}$ ) decreases with increasing the ECSF parameters and micro dimple of trapezoidal shape at operating condition. This can be attributed to the reduction in the values (16.23%) of coefficient of friction ( $\bar{\mu}$ ), having more prominent externally applied magnetic field and long chain polymer additives effects and micro dimple of trapezoidal shape. An increase in fluid layer thickness tends to lessen the coefficient of friction as the area accessible for flow increases [38]. The coefficient of friction reduces with an increase in the ECSF characteristics because the shear force depends on this pressure gradient.

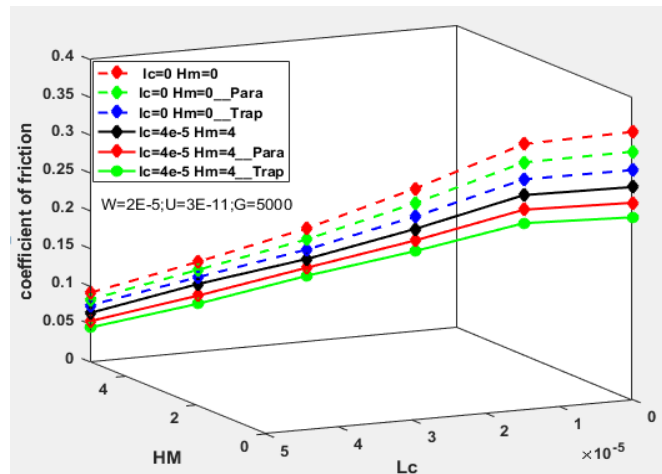


**Fig 7: Effect of ECSF parameter and different geometry of micro dimple on coefficient of friction at  $W=2 \times 10^{-5}$ ;  $U=3 \times 10^{-11}$ ;  $G=5000$**

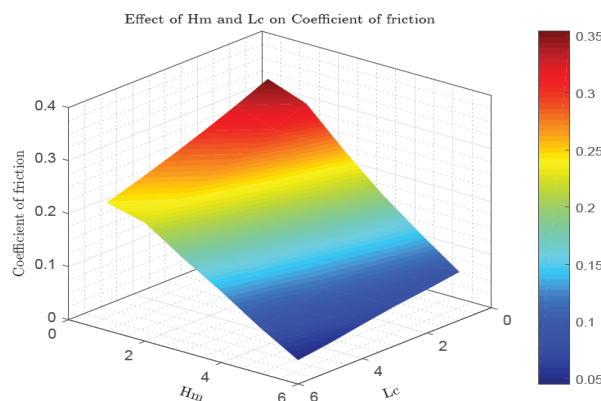


**Fig 8: Effect of ECSF parameter and different geometry of micro dimple on coefficient of friction at  $W=2 \times 10^{-5}$ ;  $U=3 \times 10^{-11}$ ;  $G=5000$ ;  $H_m=0-6$  and  $L_c = 0 - 6 \times 10^{-5}$**

## 5.2 Effect of material parameter and electrical conducting couple stress fluid parameters with micro dimples

Figure 9 and 10 shows the effect of material parameter and electrical conducting couple stress fluid parameters with micro dimples on minimum ( $H_{min}$ ) and central ( $H_{cent}$ ) fluid film thickness. For a given set of operating conditions, as depicted in Figs. 5 and 6, the  $H_{min}$  and  $H_{cent}$  fluid film thickness increases with increase in material parameter. A function of  $\alpha$  and  $E'$  is the material parameter ( $G$ ). A function of  $\alpha$  and  $E'$  is the material parameter ( $G$ ). In a physical system, as  $\alpha$  increases, the viscosity elevates as well, resulting in a thicker film. It is also observed that using micro dimples with different shapes (parabolic and trapezoidal),  $H_{min}$  and  $H_{cent}$  fluid film thickness increases significantly. Electrical conducting couple stress fluid

parameters ( $H_m=2$ ;  $l_c=2 \times 10^{-5}$ ) and trapezoidal shape of micro textures gives higher fluid film thickness over non-conducting electric fluid (NCL). Providing micro dimples, generates additional hydrodynamic pressure in localized zone as well as cavitation area in the contact surfaces. As a result of this load carrying capacity of textured contact surfaces with trapezoidal micro dimple enhance significantly compared to untextured contact surfaces. Due to the usage of trapezoidal-shaped micro-dimples in EHL line contacts,  $H_{min}$  and  $H_{cent}$  fluid film thickness have been shown to increase by a maximum of 52.36% and 59.59%, respectively. The application of an ECSF with a magnetic field and micro dimples to raise the  $H_{min}$  and  $H_{cent}$  fluid film thickness

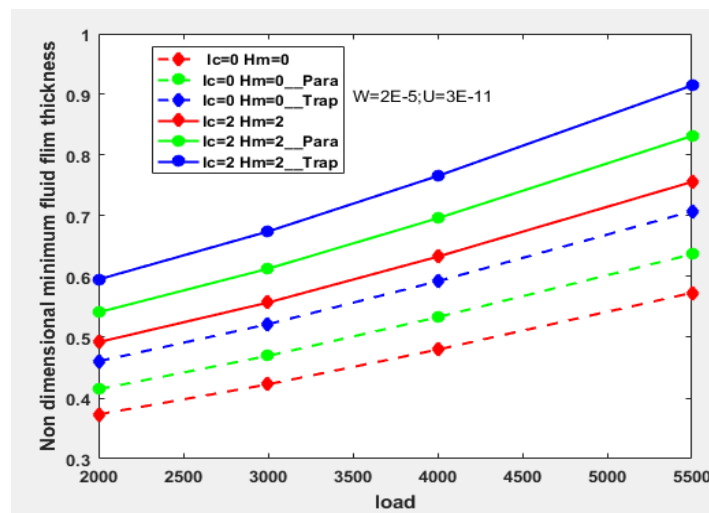


Fig 9: variation minimum fluid film thickness with material parameter at  $W=2 \times 10^{-5}$ ;  $U=3 \times 10^{-11}$

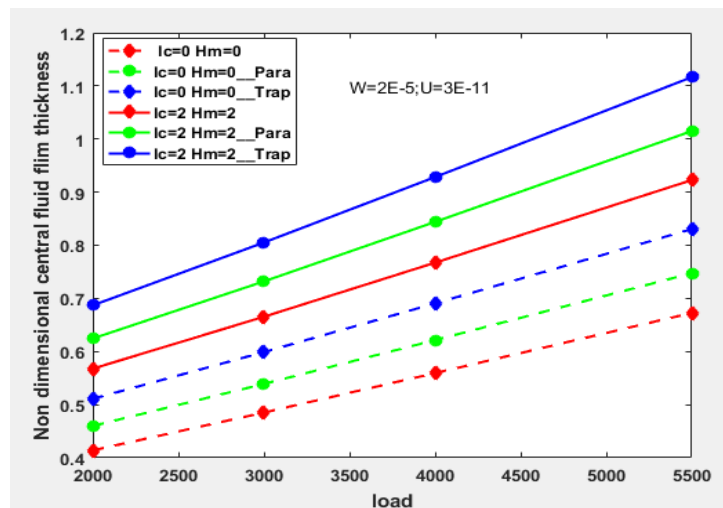


Fig 10: variation central fluid film thickness with material parameter at  $W=2 \times 10^{-5}$ ;  $U=3 \times 10^{-11}$

## 6. CONCLUSION

On the EHL line contact, the synergistic effect of an electric conducting couple stress lubricants and micro-dimples are investigated. The computationally simulated outcomes of the present investigation are summarised as follows:

1. Compared to the NCL case, the combined effects of micro dimples, electric conducting couple stress lubricants provide an increase in the performance of EHL line contacts. Moreover, these effects on the performances of EHL line contacts are more pronounced with Hartmann number, couple stress parameter and micro dimples.
2. Use of applied magnetic field, additives and micro dimple with trapezoidal shape ( $H_m=4$ ;  $l_c=4 \times 10^{-5}$ ; Trape) in conjunction results into maximum of 33.48% increase in fluid film thickness and reduce peak pressure of 22.38% compared to Newtonian lubricants.
3. Friction coefficient can be reduced i.e. 16.23 % by the use of electric conducting couple stress lubricants and micro dimples.
4. Micro dimples produce pressure rippling in EHL conjunctions and this rippling may affect the life of the contacting surfaces.
5. The current investigation shows that using electric conducting couple stress lubricants and micro dimples can significantly improve the overall performance of EHL line contacts. The rolling element's life could be increased and wear reduced as a result.

## Reference

- 1) Das N (1997) Elastohydrodynamic lubrication theory of line contacts: couple stress fluid model. *Tribology transactions* 40 (2):353-359
- 2) Raghavendra Rao R, Raja Sekhar K (2007) Effects of couple stresses and surface roughness on the film thickness of heavily loaded rollers. *Industrial Lubrication and Tribology* 59 (6):285-296
- 3) Akbarzadeh S, Khonsari M (2013) On the optimization of running-in operating conditions in applications involving EHL line contact. *Wear* 303 (1-2):130-137
- 4) Liu H, Zhu C, Sun Z, Zhang Y, Song C (2016) Coefficient of friction of a starved lubricated spur gear pair. *Journal of Mechanical Science and Technology* 30 (5):2171-2177
- 5) Xiao L, Rosen B-G, Amini N, Nilsson PH (2003) A study on the effect of surface topography on rough friction in roller contact. *Wear* 254 (11):1162-1169
- 6) Torabi A, Akbarzadeh S, Salimpour MR (2016) Mixed Thermo elastohydrodynamic lubrication analysis of finite length cam and follower mechanism. *Journal of Mechanical Science and Technology* 30 (3):1295-1303
- 7) Sarangi M, Majumdar B, Sekhar A (2005) Elastohydrodynamically lubricated ball bearings with couple-stress fluids, Part I: Steady-state analysis. *Tribology transactions* 48 (3):404-414
- 8) Saini P, Kumar P, Tandon P (2008) Surface roughness effects in elastohydrodynamic lubrication line contacts using couple stress fluid. *Proceedings of the Institution of Mechanical Engineers, Part J: Journal of Engineering Tribology* 222 (2):151-155

- 9) Menezes PL, Kailas SV (2008) Effect of surface roughness parameters and surface texture on friction and transfer layer formation in tin–steel tribo-system. *Journal of materials processing technology* 208 (1-3):372-382
- 10) Elco R, Hughes W (1962) Magnetohydrodynamic pressurization of liquid metal bearings. *Wear* 5 (3):198-212
- 11) Roberts W (1981) Tribology in nuclear power generation. *TRIBOLOGY international* 14 (1):17-28
- 12) Anwar MI, Rodkiewicz CM (1972) Nonuniform magnetic field effects in MHD slider bearing. *Journal of Lubrication Technology* 94 (1):101-105
- 13) Malik M, Singh D (1980) Analysis of finite magnetohydrodynamic journal bearings. *Wear* 64 (2):273-280
- 14) Kamiyama S (1969) Magnetohydrodynamic journal bearing (report 1). *Journal of lubrication Technology* 91 (3):380-386
- 15) Hamza E (1991) The magnetohydrodynamic effects on a fluid film squeezed between two rotating surfaces. *Journal of Physics D: Applied Physics* 24 (4):547
- 16) Maki ER, Kuzma DC, Donnelly RJ (1966) Magnetohydrodynamic lubrication flow between parallel plates. *Journal of Fluid Mechanics* 26 (3):537-543
- 17) Yu H, Huang W, Wang X (2013) Dimple patterns design for different circumstances. *Lubrication Science* 25 (2):67-78
- 18) Pettersson U, Jacobson S (2003) Influence of surface texture on boundary lubricated sliding contacts. *Tribology International* 36 (11):857-864
- 19) Costa H, Hutchings I (2007) Hydrodynamic lubrication of textured steel surfaces under reciprocating sliding conditions. *Tribology International* 40 (8):1227-1238
- 20) Marian V, Kilian M, Scholz W (2007) Theoretical and experimental analysis of a partially textured thrust bearing with square dimples. *Proceedings of the Institution of Mechanical Engineers, Part J: Journal of Engineering Tribology* 221 (7):771-778
- 21) Etsion I (2013) Modeling of surface texturing in hydrodynamic lubrication. *Friction* 1 (3):195-209
- 22) Cupillard S, Glavatskih S, Cervantes M (2008) Computational fluid dynamics analysis of a journal bearing with surface texturing. *Proceedings of the Institution of Mechanical Engineers, Part J: Journal of Engineering Tribology* 222 (2):97-107
- 23) Thakre GD, Sharma SC, Harsha S, Tyagi M (2016) A theoretical study of ionic liquid lubricated  $\mu$ -EHL line contacts considering surface texture. *Tribology International* 94:39-51
- 24) Sinhasan R, Jain S (1984) Lubrication of orifice-compensated flexible thrust pad bearings. *Tribology international* 17 (4):215-221
- 25) Ramanaiah G, Sarkar P (1978) Squeeze films and thrust bearings lubricated by fluids with couple stress. *Wear* 48 (2):309-316
- 26) Jin Z, Dowson D (1997) A general analytical solution to the problem of microelastohydrodynamic lubrication of low elastic modulus compliant bearing surfaces under line contact conditions. *Proceedings of the Institution of Mechanical Engineers, Part C: Journal of Mechanical Engineering Science* 211 (4):265-272
- 27) Dowson D, Higginson G (1959) A numerical solution to the elasto-hydrodynamic problem. *Journal of Mechanical Engineering Science* 1 (1):6-15

- 28) Roelands C, Vlugter J, Waterman H (1963) The viscosity-temperature-pressure relationship of lubricating oils and its correlation with chemical constitution. *Journal of Basic Engineering* 85 (4):601-607
- 29) Lu H, Berzins M, Goodyer C, Jimack P (2005) High-order discontinuous Galerkin method for elastohydrodynamic lubrication line contact problems. *International Journal for Numerical Methods in Biomedical Engineering* 21 (11):643-650
- 30) Lu H, Berzins M, Goodyer C, Jimack P, Walkley M (2006) Adaptive high-order finite element solution of transient elastohydrodynamic lubrication problems. *Proceedings of the Institution of Mechanical Engineers, Part J: Journal of Engineering Tribology* 220 (3):215-225
- 31) Goodyer CE, Berzins M, Jimack PK, Scales L (2006) A grid-enabled problem solving environment for parallel computational engineering design. *Advances in Engineering Software* 37 (7):439-449
- 32) Reddy JN (1993) *An introduction to the finite element method, vol 2. vol 2.2.* McGraw-Hill New York,
- 33) Hamrock BJ, Jacobson BO (1984) Elastohydrodynamic lubrication of line contacts. *ASLE transactions* 27 (4):275-287
- 34) Dowson D Paper 10: Elastohydrodynamics. In: *Proceedings of the Institution of Mechanical Engineers, Conference Proceedings, 1967. vol 1.* SAGE Publications Sage UK: London, England, pp 151-167
- 35) Daliri M, Jalali-Vahid D, Rahnejat H (2015) Magneto-hydrodynamics of couple stress lubricants in combined squeeze and shear in parallel annular disc viscous coupling systems. *Proceedings of the Institution of Mechanical Engineers, Part J: Journal of Engineering Tribology* 229 (5):578-596
- 36) Lin J-R, Chu L-M, Hung C-R, Wang P-Y (2013) Derivation of two-dimensional couple-stress hydromagnetic squeeze film Reynolds equation and application to wide parallel rectangular plates. *Meccanica* 48 (1):253-258
- 37) Lin J-R (2010) MHD steady and dynamic characteristics of wide tapered-land slider bearings. *Tribology International* 43 (12):2378-2383
- 38) Jadhav, S., Thakre, G. D., & Sharma, S. C. (2018). Numerical modeling of elastohydrodynamic lubrication of line contact lubricated with micropolar fluid. *Journal of the Brazilian Society of Mechanical Sciences and Engineering*, 40,1-17.
- 39) Kumar P, Jain S, Ray S (2008) Influence of polymeric fluid additives in EHL rolling/sliding line contacts. *Tribology International* 41 (6):482-492.